A Structure Planning Approach for Semi-Rigid Base Asphalt Advance Pavement That Relies On Optimization of Elasticity

Yogesh Chauhan[1], Satish Parihar[2]
M. Tech Scholar Civil Engineering FET, Rama University Uttar Pradesh 209217
Associate Professor Civil Engineering FET, Rama University Uttar Pradesh 209217
Email. yogeshkrishna349@gmail.com, satishparihar.fet@ramauniversity.ac.in

Abstract:
The early damage of the semi-rigid base asphalt pavement is related to the pavement structure modulus's unreasonable matching. In this study, three typical pavement structures were selected to analyze the pavement structures' influence on the pavement service life. A three-dimensional finite element pavement structure model was established. The independent variables are subgrade modulus, base course modulus, and subbase modulus. The deflection, the bottom tensile stress, and maximum shear stress were chosen as the evaluation indexes. The effect of the modulus on the mechanical response of the pavement structure was analyzed. The optimal modulus combination of the pavement structure was determined through multi-factor range analysis. The mechanical response and fatigue life before and after the optimization pavement structure were compared. The results showed that the field measured modulus of Structure 1 and 2 was higher than the design modulus. Moreover, while the modulus of base course and subbase course was increased, the deflection gradually reduced. The base course's bottom tensile stress and the subbase were increased, and the maximum shear stress was basically unchanged. After the modulus combination optimized pavement structure, the mechanical response was significantly reduced. The fatigue life based on the deflection and bottom tensile stress, and the laboratory normalized fatigue equation were significantly increased. By the combination of fatigue performance of pavement materials and pavement structure, it was possible to provide an effective optimization method for the design of semi-rigid base asphalt pavement in this research work.
Keywords: Modulus optimization Semi-rigid layers Structure Design Asphalt Pavement Fatigue life

1.0 Introduction

The semi-rigid base asphalt pavement has the advantages of high rigidity, high strength, and higher bearing capacity. So, it is widely used on high-grade highways. However, most of the semi-rigid base asphalt pavement has experienced severe functional degradation and structural damage before reaching the designed service life [14]. For example, in China, about 60% of expressway asphalt pavements show apparent structural damage after 10 to 12 years, and 17% are visible after 6 to 8 years [1–3]. It has caused substantial economic losses and adverse social impacts [39]. These damages are related to construction quality and overload, and also they are associated with the structural design's theoretical system and structural combination design [4–6]. In the pavement structure combination design, the overall influence of sub- grade, base course, and surface is considered [40]. Reasonable structural forms are adopted. The rationally structural parameters are determined. This combination design conforms to the design idea of the long-life asphalt pavement structure [7–10]. It has important practical significance in improving the service life of semi-rigid base asphalt pavement. The semi-rigid base asphalt pavement is a potential long-life pavement, which attracted widespread attention from scholars [11–14]. Zhao et al. designed long-life asphalt pavement through the design of the pavement structure, pavement material selection, and construction quality control [15]. Luo et al. analyzed the influence of structural parameters on the mechanical behavior of asphalt pavement [16]. For different semi-rigid base course moduli, Zhang et al. analyzed the trend of the change of multiple evaluation indexes with the modulus [17]. It was found that a too large value of base course modulus will lead to rutting of the road surface and reduce the fatigue life of the surface course. A too small value of base modulus did not provide sufficient strength. Li et al. established a three-dimensional finite element pavement structure and analyzed the mechanical response when the base modulus varies [18]. It showed that the increase in the base course' modulus could reduce the bottom tensile strain and improve the fatigue. life of the asphalt pavement. Ma et al. revealed the influence of the base modulus on pavement rutting, shear stress, and fatigue life [19]. For instance, if the base modulus is too large, it increased the rut depth of the surface course and reduced the pavement's fatigue life. It is reasonable to control the modulus of the base course in the range of 1200 MPa ~ 1600 MPa. Zhou et al. used BISAR software to perform the mechanical sensitivity analysis of the changes in material mechanical parameters and structural geometric parameters on the pavement structure.

It showed that increasing the thickness and stiffness of the surface course or base course could reduce the deflection and the bottom tensile stress [20]. Assogba et al. found that the interlayer adhesion conditions, vehicle speed, and axle load amplitude have an impact on the fatigue properties of the pavement [21]. The model which can predict the nonlinear characteristic distribution of temperature was established. Ma et al. selected traffic volume, pavement thickness, elastic modulus, and vehicle load as the influencing parameters of asphalt pavement structure design [22]. The deflection, stress in the bottom layer, and subgrade top compression strains are used as control indicators. The reliability anal- ysis of the semi-rigid base asphalt pavement is conducted. It was found that increasing the subgrade rebound modulus and base course thickness could improve the reliability of the semi-rigid base asphalt pavement. To sum up, in the design of the pavement structure, there is more research on the mechanical response of a single base modulus parameter to the semi-rigid base pavement structure. Instead, there is less research on the combined design of pavement structure modulus. However, structural modulus combination design has a significant impact on the service life.of the pavement [23–26]. So, it is necessary to carry out a balanced and coordinated design of the modulus in the semi-rigid base asphalt pavement structure.

Based on this premise, the authors developed a finite element model to simulate the mechanical response of semi-rigid base asphalt pavements according to the design modulus and the field measured modulus. Orthogonal experiments were used to select the reasonable modulus parameters of the semi-rigid base asphalt pavement structure. Thereby, the optimal pavement structure was determined. On this basis, the fatigue life obtained by using inverse calculation of deflection and bottom tensile stress, and the prediction based on the normalized fatigue equation were compared and analyzed. The flowchart of the schematic structure in this research is shown in Fig. 1

2.0 Methodology / Hypothesis

2.1 Finite element model

In this paper, the pavement structure model size is 10 m length × 10 m width × 10 m depth. There is no displacement at the model's bottom and sides, which is wholly constrained. The top surface of the model is

contact-free. The contact between layers is considered to be completely continuous. The element type is 3D 8nodal elements (C3D8R) [27]. the closer to the top, the mesh division is concentrated when the model is established. That is to say, the farther away from the load-acting area, the division of elements gradually becomes sparse [28–30].

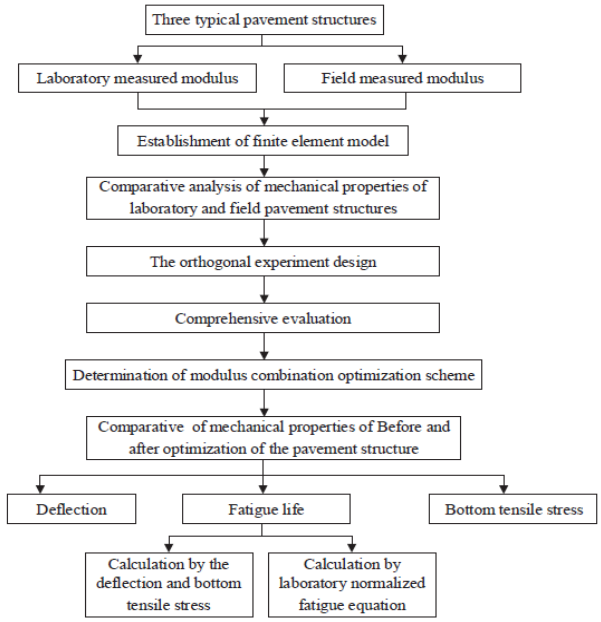

Fig. 1. The flowchart of the schematic structure.

For pavement structure 1, the upper layer, the middle layer, and the lower layer are subdivided by 4, 5, 5, respectively. The base course is subdivided by 12, and the subbase is subdivided by 5. The cushion is subdivided by 4. The subgrade is subdivided by 20.

For pavement structure 2, the upper layer, the middle layer, and the lower layer are subdivided by 4, 5, 5, respectively. The base course is subdivided by 12, and the subbase is subdivided by 5. The subgrade is subdivided by 20.

For pavement structure 3, the upper layer, the middle layer, and the lower layer are subdivided by 4, 5, 5, respectively. The base course is subdivided by 12, and the subbase is subdivided by 5. The subgrade is subdivided by 20. The three-dimensional finite element pavement structure model is shown in Fig. 2.

2.2. Load form

This paper calculates the driving load using a standard double axle load of 100KN and a tire pressure in 0.707 MPa. The approximate shape of the actual contact area of each tire can be composed of one rectangle and two semicircles. Therefore, the real contact area can be expressed by Eq. (1).

$$A_c = \pi(0.3L)^2 + (0.4L)(0.6L) = 0.5227L^2$$

$$A_c = 25 \times 10^3 / 0.707 = 35361\text{mm}^2$$

$$L = \sqrt{\frac{A_c}{0.5227}}$$

Here: *Ac* is the actual contact area between the tire and pavement. *L* is the contact length between the tire and pavement. The shape of the tire acting on the road surface

is not circular. It is closer to the rectangle, and the rectangular characteristics are more evident as the axle load increases. Therefore, the grounding shape of the tire in this paper adopts a double rectangle instead of the double circle diagram of the dual wheel. The contact area can be further simplified to a single rectangular of equal width. The rectangle's length is $0.8712 \times L$, the breadth is $0.6 \times L$, as shown in Fig. 2. The contact area can be calculated by utilizing the load on each tire and the tire pressure, which can be obtained from Eq. (2). Then the contact length can be obtained from Eq. (3). The L is 260 mm. The equivalent contact area between the tire and pavement and load application diagram is shown in Fig. 3.

Fig. 2. The three-dimensional finite element model of the pavement structure.

3. Research scheme

3.1. Pavement structure parameters

The parameters of three typical pavement structures are shown in Table 1. The 2.5 MPa, 3.5 MPa, and 4.5 MPa values are the unconfined compression strength of cement stabilized macadam at 7 days in the laboratory. When calculating the deflection, the design modulus is the compression rebound modulus of the mixture at 20 ◦C. When calculating the bottom tensile stress and the maximum shear stress, the design modulus is the compression rebound modulus of the mixture at 15 ◦C [31].

3.2. Orthogonal experiment design

Based on the results of a comparative study of the design modulus and the field measured modulus, the asphalt layer did not play the role of the main bearing layer in the structural stress [32]. So, the selection of the asphalt layer parameters is the same as the original design scheme. The structure below the asphalt layer is the primary bearing layer, so its modulus is chosen to be different in the orthogonal analysis. Structure 1 uses the base course, subbase, cushion layer, and subgrade modulus as the independent variables. Structures 2 and 3 use the base course, subbase, and subgrade modulus as the independent variables. For the three structure types, all use the deflection, bottom tensile stress of each structural layer, and maximum shear stress as the evaluation indexes. To optimize the structural layer modulus combination, the L9 (34) orthogonal analysis table was used to carry out the four-factor and three-index orthogonal test design. Orthogonal test factors and levels are shown in Table 2, where A is the subgrade modulus, B is the cushion course modulus, C is the subbase modulus, and D is the base course modulus. The orthogonal test schemes are shown in Table 3.

3.3. Modulus test method

3.3.1. Field modulus measurement

According to the Specifications for Design of Highway Asphalt Pavement and AASHTO T0944, the resilient modulus was measured by the Beckman beam method. The axle type of the standard vehicle is a double axle truck with four wheels on both sides of the rear axle. The main parameters of a standard vehicle are shown in Table 4.

The Beckmann beam reflectometer with a length of 5.4 m is used to produce deflection. The front and rear arms are 3.6 m and 1.8 m, respectively. The deflection is measured with a dial indicator. The specific steps are as follows:

(1) The measuring points were arranged in the measured section. According to the Fig. 4, the distance between the measuring points was arranged within the range of 2 m × 1 m in the middle, and 23 points were measured.

(2) The rear wheel clearance of the standard vehicle was aligned to 3 ~ 5 cm after the measuring point.

(3) The deflect meter was inserted into the gap between the standard vehicle's rear wheels, which is consistent with the direction of the standard vehicle. The measuring head of the deflect meter was placed on the measuring point. The dial indicator was installed on the measuring rod of the deflect meter, which should be adjusted to zero.

(4) The standard vehicle moved slowly. The dial indicator continues to rotate forward as the deformation increases. When the hand turns to the maximum value, the value at this time is recorded as $L1$. The standard vehicle is still moving forward, and the dial indicator's hands turn in the opposite direction. After the standard vehicle drives out of the deflection radius, it stops. The final value of the dial indicator was recorded as $L2$. The forward speed of the standard vehicle was 5 km/h.

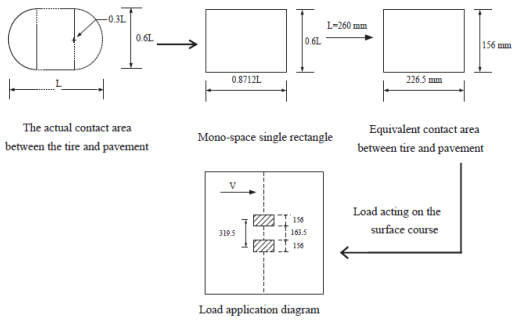

Fig. 3. The contact area and load application diagram

Table 1
Pavement structure parameters.

Pavement structure	Structural layer	Material type	Structural thickness (cm)	Modulus for deflection (MPa)	Modulus for stress (MPa)	Poisson's ratio
1	Upper layer	AC-13C	4	1300	1900	0.25
	Middle layer	AC-20C	6	1200	1800	0.25
	Lower layer	AC-25C	8	900	1300	0.25
	Base course	Cement stabilised macadam(3.5 MPa)	36	1200	3300	0.25
	Subbase	Cement stabilised macadam (2.5 MPa)	20	800	2700	0.25
	Cushion	Graded broken stone	20	300	300	0.25
	Subgrade	–	–	40		0.35
2	Upper layer	AC-13C	4	1400	2000	0.25
	Middle layer	AC-20C	6	1200	1800	0.25
	Lower layer	AC-25C	8	1000	1200	0.25
	Base course	Cement stabilised macadam (3.5 MPa)	36	1500	3500	0.25
	Subbase	Cement stabilised macadam (2.5 MPa)	20	1300	3100	0.25
	Subgrade	–	–	40		0.35
3	Upper layer	SMA-13C	4	1200	1800	0.25
	Middle layer	AC-20C	6	1000	1600	0.25
	Lower layer	AC-25C	8	800	1000	0.25
	Base course	Cement stabilised macadam (4.5 MPa)	36	1500	3500	0.25
	Subbase	Cement stabilised macadam (3.5 MPa)	20	1300	3200	0.25
	Subgrade	–	–	40		0.35

(5) The deflection value of the measuring point was calculated as follows:

$$l_1 = (L_1 - L_2) \times 2 \quad (4)$$

where l_1 is the deflection of the measuring point; L_1 is the maximum value of the dial indicator; L_2 is the final value of the dial indicator. The deflection of 23 measuring points can be obtained from the above. The mean value, standard deviation, and coefficient of variation were calculated according to the following formula.

$$\overline{L} = \frac{\sum_{i=1}^{23} l_i}{N} \quad (5)$$

$$S = \sqrt{\frac{\sum (l_i - \overline{L})}{N-1}} \quad (6)$$

$$C_v = \overline{L}/S \quad (7)$$

The final deflection value was calculated according to the following equation to calculate the resilient modulus:

Table 2
Orthogonal test $L_9(3^4)$ factor level table.

Structure	Level	Subgrade modulus (A)/MPa	Cushion course modulus(B)/MPa	Subbase modulus (C)/MPa		Base course modulus (D)/MPa	
				Calculate deflection	Calculate stress	Calculate deflection	Calculate stress
1	1	30	200	700	2500	1100	3100
	2	40	300	800	2700	1200	3300
	3	50	400	900	2900	1300	3500
2	1	30	"	1100	3000	1500	3500
	2	40	"	1200	3200	1600	3800
	3	50	"	1300	3400	1700	4100
3	1	30	"	1200	3000	1500	3500
	2	40	"	1300	3200	1600	3800
	3	50	"	1400	3400	1700	4100

Table 3 The orthogonal test schemes of the structure modulus optimization combination.

Test number	Column number			
	A	B	C	D
1	1	1	1	1
2	1	2	2	2
3	1	3	3	3
4	2	1	2	3
5	2	2	3	1
6	2	3	1	2
7	3	1	3	2
8	3	2	1	3
9	3	3	2	1

Table 4
The main parameters of standard vehicle.

Standard axle load rating	BZZ-100	Unit
Standard rear axle load	100	kN
Double wheel load on one side	50	kN
Tire inflation pressure	0.707	MPa
Equivalent circle diameter of single wheel pressure transmitting surface	21.30	cm

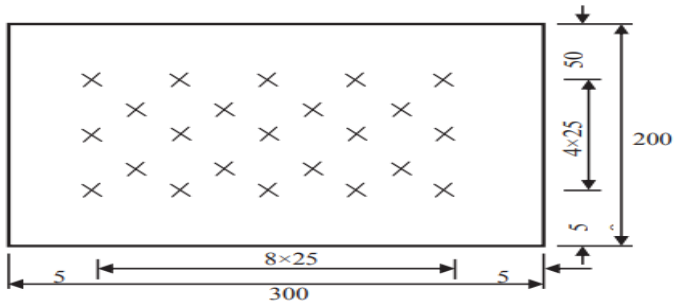

Fig. 4. Layout of measuring points.

$$L = \overline{L} + S \quad (8)$$

The final deflection value was calculated according to the following equation to calculate the resilient modulus:

$$E = \frac{2p\delta}{L}(1-\mu^2)a$$

Here: E is the resilient modulus. p is the average vertical load of the standard vehicle wheels. δ is the equivalent circle radius of single wheel pressure transmitting surface. L is the deflection value. μ is the Poisson's ratio of measuring layer material. a is the deflection coefficient, which is 0.712.

3.3.2. Laboratory modulus measurement

According to the ASTM D 1074 and AASHTO T167, the compressive strength test was conducted to obtain the mean compressive strength of the asphalt mixture. The strength was recorded as P. Load to 0.2P at the speed of 2 mm/min for preloading and hold for 1 min. Record the original readings of two dial indicators after unloading. Load to 0.1P at the speed of 2 mm/min, immediately record the dial indicator reading and the actual load number and unload at the same speed back to zero. After the specimen rebounds deformation for the 30 s, record the dial indicator reading again. The difference between the two loading and unloading readings is the rebound deformation of the specimen under this load. Then the next loading and unloading process is carried out in turn, and the rebound deformation of all levels of the load is obtained. According to the following formula, the compressive resilient modulus of asphalt mixture specimen can be calculated [31].

$$q_i = \frac{4P_i}{\pi d^2}$$

$$E' = \frac{q_5 \times h}{\Delta L_5}$$

where q_i is the pressure under various test loads. Pi is the various test loads. d is the diameter of specimen. E' is the uniaxial compression rebound modulus. h is the axis height. ΔL5 is the rebound deformation of the specimen under the fifth test load.

4. Result analysis

4.1. Comparison of mechanical response based on design modulus and field measured modulus

The compression rebound modulus in the field can be measured by Benkelman Beam. In order to evaluate the effect of modulus on the mechanical response, the representative values of the field measured results were calculated by using Eqs. (12) and (13) [31]. Table 5 shows the field measured results and representative values of the modulus.

$$E_{os1} = \overline{E_0} - Z_a S$$

$$E_{os2} = \overline{E_0} + Z_a S$$

Here: Eos1 is the representative value of modulus for deflection. Eos2 is the representative value of modulus for stress. E0 is the average value of the field measured modulus. Za is the guarantee rate coefficient, which is 2.0. S is the mean square error of the field measured modulus.

According to the representative values of the modulus of the base course and subbase, the other structural parameters were unchanged. The mechanical response for the three type structures was calculated by the finite element. The calculation results were shown in Fig. 5.

Table 5
Field measured results.

Structure	Structural layer	Measured modulus (MPa)			A representative value of the modulus (MPa)	
		Average value	Mean square error	Coefficient of variation	Modulus for deflection (MPa)	Modulus for stress(MPa)
1	Base course	5897	1046.60	0.1774	3803.80	7990.20
	Subbase	4595	835.87	0.1818	2923.26	6266.74
2	Base course	5945	1183.51	0.1990	3577.98	8312.02
	Subbase	4389	982.74	0.2238	2423.52	6354.48
3	Base course	2155	421.03	0.1953	1312.94	2997.06
	Subbase	1698	256.09	0.1507	1185.82	2210.18

It can be noticed that for Structure 1, the field measured modulus of the base course and subbase increases. The bottom tensile stress of the base course and subbase increases when its modulus increase. This means that the structure layer stiffness is higher; the corresponding structural layer will bear more loads. The tensile stresses are by definition positive, and compressive stresses are negative. The bottom layer of the upper layer, middle layer, and the lower layer is under pressure. The maximum shear stress of the surface course does not change with the change of the modulus of the base course and subbase, which is because the maximum shear stress is mainly affected by the modulus and thickness of the surface course. The deflection under the design modulus is 0.3627 mm, while under the field measured modulus is 0.2746 mm. The deflection decreases with the increase of the base course and subbase modulus. For Structure 2 and Structure 3, the field measured modulus of the base course and subbase is not much different from the design modulus. So, the calculation results of all evaluation indexes are also similar.

It can be seen by comparing and analyzing the three type pavement structures that there is an absolute difference between the structural layer modulus design value and the field measured value. The field modulus of the base course and subbase is higher than the design modulus. It leads to a decrease in deflection and the increase of bottom tensile stress. Thereby it leads to the impact on pavement performance. Then, the orthogonal experiment is used to analyze the influences in this paper.

4.2. Orthogonal experiment results

4.2.1. Significance analysis of range values

The size of the range directly reflects the degree of influence of the independent variable venations on the evaluation index. Higher range indicates that the impact of the independent variables on the evaluation index is more significant. Thus, it has an intuitive understanding of the importance of various elements in road design. The range analysis of Structure 1 is shown in Fig. 6. The left axis is the mechanical response value, which is represented by the line graph. The right axis is the range, which is represented by the column graph. The range is the difference between the maximum and minimum evaluation index value corresponding to a certain level. The range analysis graph of Structure 2 and Structure 3 are similar to that of Structure 1, which is shown in Appendix A.

For Structure 1, Fig. 6a shows that the order of influence of each factor on the deflection is as follows: subgrade modulus > cushion course modulus > base course modulus > subbase modulus. The influence of subgrade modulus on deflection is more significant than other factors. Fig. 6b shows that for the maximum shear stress, it is generally not significantly affected by the modulus of the structural layer. The maximum shear stress has almost no change under the influence of various independent variables. Fig. 6c and 6d show that the value of the lower layer, middle layer, and upper layer tensile stress are all negative under the influence of the base course, subbase, cushion course, subgrade modulus. The results indicate that the three asphalt layers will not undergo flexural fatigue damage at the bottom of the structural layer. In other words, bending tensile stress at

the bottom of the structural layer occurs only at the bottom of the semi-rigid base course and subbase. Fig. 6e shows that for the bottom tensile stress of the subbase course, the order of importance of the various elements is as follows: cushion course modulus > subgrade modulus > subbase modulus > base course modulus. For the bottom tensile stress of the base course, the order of importance of the various elements is as follows: the base course modulus > the subbase modulus > the subgrade modulus = cushion course modulus. In the case of Structure 2, for deflection, the order of influence of each independent variable is as follows: subgrade modulus > base course modulus > subbase modulus. For the bottom tensile stress of the subbase, the order of importance of the independent variables is as follows: subgrade modulus > subbase modulus > base course modulus. For the bottom tensile stress of the base course, the rule of the impact of the independent variables is as follows: base course modulus > subbase modulus > subgrade modulus. The bottom tensile stresses of the asphalt upper layer, middle layer, and lower layer are all negative under the influence of the base course modulus, subbase modulus, and subgrade modulus. This fact indicates that the bottom of the upper layer, middle layer, and lower layer is under pressure. So, all three asphalt layers will not undergo bending tensile fatigue failure at the bottom of the surface structure layer. As for the maximum shear stress, it barely changes under the influence of various factors.

In the analysis of Structure 3, for deflection, the order of influence of each independent variable is as follows: subgrade modulus > base course modulus > subbase modulus. For the bottom tensile stress of the subbase, the order of the impact degree of each independent variable is as follows: subgrade modulus > subbase modulus > base course modulus. For the bottom tensile stress of the base course, the law of influence of each independent variable is as follows: base course modulus > subbase modulus > subgrade modulus. For the maximum shear stress and the bottom tensile stress of the upper layer, middle layer, and lower layer, the results obtained are similar to those of Structure 2. A comprehensive analysis of the three typical structures shows that increasing the subgrade modulus can significantly reduce deflection. The graded broken stone cushion layer is set between the subbase and the subgrade, which can improve the state of the bottom tensile stress of the subbase. On the other hand, the bottom tensile stress of the subbase is also affected by the base course and subgrade modulus. As for the bottom tensile stress of the base course, its state is significantly affected by the modulus of the base course itself, and the subbase's modulus. The bottom tensile stress increases with the increase of the base modulus. Therefore, to prevent the bending and tensile fatigue failure of the bottom layer in the semi-rigid base asphalt pavement, the modulus of the base course should be appropriately reduced. It can reduce the bending tensile stress of the structural layer bottom. In short, attention to subgrade treatment plays an essential role in improving deflection indicators. Properly reducing the modulus of the semi-rigid base course can reduce the bending tensile stress at the bottom of the structural layer and can effectively extend the service life of the asphalt pavement. The modulus of each structural layer needs to have a reasonable match to meet the force coordination of the pavement structure.

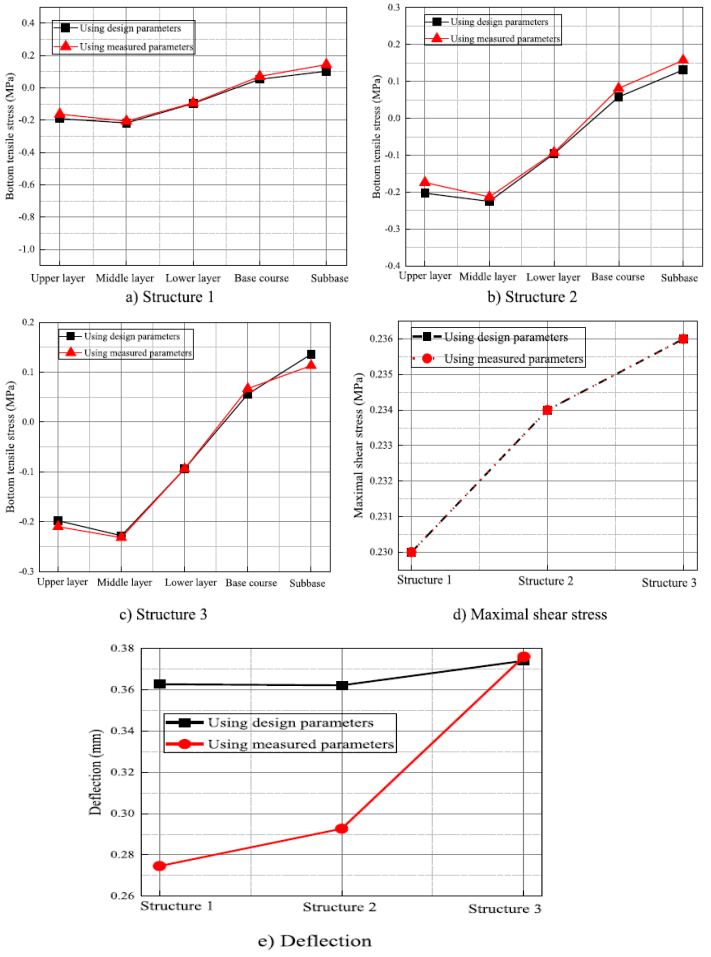

Fig. 5. The calculation results of the pavement structure.

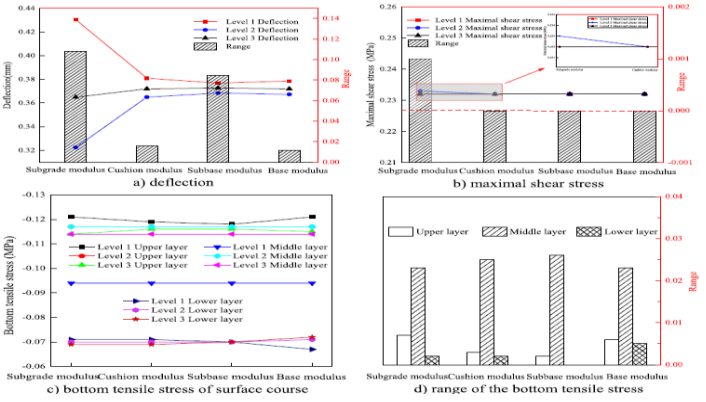

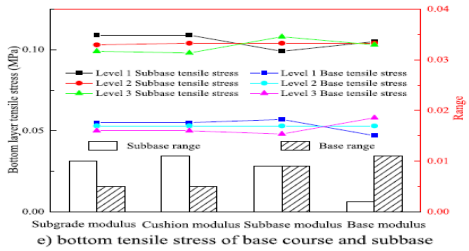

Fig. 6. The range analysis results of Structure 1

4.2.2. Level influence optimal combination analysis

The multi-factor range analysis is carried out through the orthogonal experiment results. The first value of each evaluation index is used as the reference value, which is determined as 100 points. The score of the remaining value is calculated by using the Eq. (14). The comprehensive score is the sum of the scores of the different evaluation indicators. The deflection, bottom tensile stress of each structural layer, and maximal shear stress of the surface course are to be taken into account. The value of the evaluation indicators is smaller, the deflection, the bottom tensile stress, and the maximal shear stress are lower. Therefore, the comprehensive score is lower, and the corresponding pavement structure is safer. The calculation results are shown in Fig. 7.

$$S_i = 100 \cdot \frac{v_i}{v_0}$$

where: v_i is the calculation indicator value of the group i. v_0 is the calculation indicator value of the group 1. Fig. 7a is the comprehensive score of Structure 1. Taking the subgrade modulus as an example, the score of level 1 is 700, which is used as the reference score. The level 2 score is 695, and that of level 3 is 670. The lowest score is the third level. In other words, the pavement structure is the most reliable under level 3 of the subgrade modulus. Thus, level 3 of the subgrade modulus is selected to be the optimization value of the subgrade modulus. Because the subgrade modulus is represented by A in the orthogonal test factors, the subgrade modulus under level 3 can be represented by A3. By comparing the remaining evaluation indicators, the best combination of Structure 1 is determined as A3B3C1D1.

According to the above method, Table 6 shows the comprehensive score of three typical pavement structures and the best combination. The deflection increases with the increase of the base course modulus. But from the optimal result, the base course modulus decreases appropriately to correspond to the other structural layer modulus. It can improve the mechanical performance of the entire road surface. On the other hand, it can achieve the purpose of stiffness gradient and deformation coordination. The method comprehensively considers the influence of each independent variable on each other; meanwhile, it considers each evaluation index. The optimal combination schemes can be determined by the comprehensive score.

In the pavement structure design, the base course modulus and the subgrade modulus play a key role. It is relatively feasible to control the base course modulus properly and the subgrade modulus to effectively

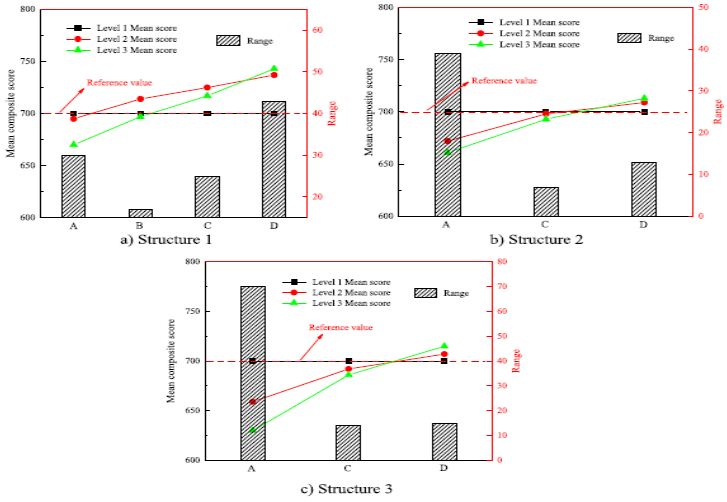

Fig. 7. The comprehensive score of three typical pavement structure.

Table 6
The best combination of three typical pavement structures.

Pavement structure	Factor	Score of level 1	Score of level 2	Score of level 3	Range between the score	Best combination
Structure 1	A	700	695	670	30	A3
	B	700	714	697	17	B3
	C	700	725	717	25	C1
	D	700	737	743	43	D1
Structure 2	A	700	672	661	39	A3
	C	700	698	693	7	C3
	D	700	709	713	13	D1
Structure 3	A	700	659	630	70	A3
	C	700	692	686	14	C3
	D	700	707	715	15	D1

reduce the deflection and the bottom tensile stress. It is not possible to select the structural layer modulus according to the material alone. It is necessary to consider the mutual influence between the structural layers. Each evaluation index should be comprehensively taken into account. Then, the reasonable modulus combination is determined.

4.3. Determination of modulus combination optimization scheme

Learning the optimal combination of structural layer modulus for different pavement structure types is an essential theoretical support for solid application engineering. The comprehensive score is the smallest. The durability of the pavement structure is best. The corresponding structural parameters are optimized structural parameters. According to the multi-factor range analysis, the optimal pavement structure is shown in Table 7. The

following conclusions can be drawn from Table 7. When

Table 7
The asphalt pavement structure optimized parameters.

Pavement structure	Structure layer	Modulus (MPa)			Thickness (cm)
		Deflection	Bottom tensile stress	Maximal shear stress	
1	Upper layer	1300	1900	800	4
	Middle layer	1200	1800	700	6
	Lower layer	900	1300	600	8
	Base course	1100	3000	3000	36
	Subbase	700	2500	2500	20
	Cushion layer	400	400	400	20
	Subgrade	50			
2	Upper layer	1400	2000	750	4
	Middle layer	1200	1800	700	6
	Lower layer	1000	1200	600	8
	Base course	1500	3500	3500	36
	Subbase	1300	3400	3400	20
	Subgrade	50			
3	Upper layer	1200	1800	750	4
	Middle layer	1000	1600	700	6
	Lower layer	800	1000	600	8
	Base course	1500	3500	3500	36
	Subbase	1400	3400	3400	20
	Subgrade	50			

calculating the deflection, the optimal modulus of the base course and subbase of Structure 1 is 1100 MPa and 700 MPa, respectively, that of the Structure 2 is 1500 MPa and 1300 MPa, respectively, and that of the Structure 3 is 1500 MPa and 1400 MPa, respectively. When calculating the stress, the optimal modulus of the base course and subbase of Structure 1 is 3000 MPa, and 2500 MPa, respectively, and those of Structure 2 and Structure 3 both are 3500 MPa and 3400 MPa respectively. The optimal modulus of the subgrade of the three type structures is 50 MPa. The graded broken stone with a particular thickness set is in Structure 1, which can improve the deformation and force coordination of pavement structure. Meanwhile, the base course modulus and the subbase modulus can be appropriately reduced due to this. It can be seen from the optimal scheme that the value of the modulus related to base course and subbase, if it increases from a range of values, it does not produce a better performance. The modulus of the base course and subbase should be reduced to coordinate with the modulus of other structural layers. It can achieve the goal of improving the stress state inside the asphalt pavement structure.

5. Comparison of mechanical properties before and after optimization of the pavement structure

5.1. Mechanical responses before and after optimization of the pavement structure

Different pavement structures have different mechanical response results under standard axle load. Furthermore, the corresponding pavement structure will have different fatigue lives. In this paper, to verify the reliability of the optimization results, the mechanical response of the before and after optimization pavement was analyzed. Each structure's deflection and bottom tensile stress under the standard axle load was calculated. The results are shown in Fig. 8. For Structure 1, Structure 2, and Structure 3, compared with the original design structure, the deflection value after the optimization of pavement structure reduced its value by 20.8%, 19.0%, 19.8%, respectively. And the maximum bottom tensile stress of the base course decreased by 9.8%, 15.5%, and 12.4%, respectively. From the related research results [33], it can be found that with the increase of the modulus, the horizontal tensile stress in the driving direction of the subbase decreases significantly, and the horizontal tensile strain decreases gradually.

Therefore, compared with the original pavement structure, the optimized pavement structure's modulus increases, and the deflection and bottom tensile stress decrease. The pavement structure adopts a load-transmitting structure, which mainly transfers the load and supports the load as a supplement.

5.2. Fatigue life before and after optimization of the pavement structure

5.2.1. Back-calculated calculation results of fatigue life based on deflection and bottom tensile stress

The deflection and the bottom tensile stress are determined by using the subsection 4.1. The cumulative equivalent axis loads of the asphalt pavement structure is back-calculated by the deflection, which is the fatigue life [31]. The expression is as follows.

$$N_e = \left(\frac{l_s}{600A_c \cdot A_s \cdot A_b}\right)^{\frac{1}{-0.2}} \tag{15}$$

The cumulative equivalent axis loads of the asphalt pavement structure is back-calculated by utilizing the bottom tensile stress, which is as follows.

$$N_e = \left(\frac{\sigma_{sp} \cdot A_c}{\sigma \cdot A}\right)^{\frac{1}{B}} \tag{16}$$

In the above formula: *Ne* is the cumulative equivalent axis loads, time; *ls* is the deflection, mm. *Ac* is the road grade coefficient, which is

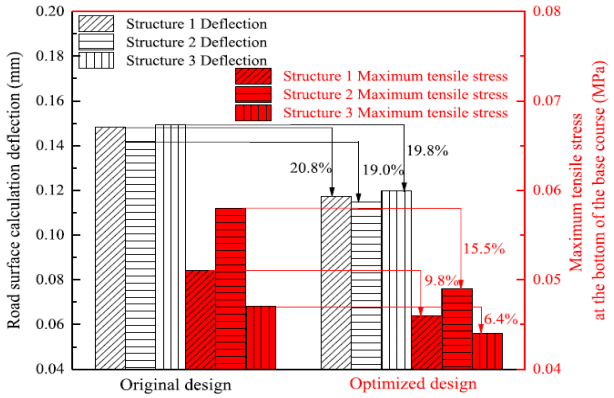

Fig. 8. Comparison of the mechanical response before and after optimization pavement structure.

road structure type coefficient, which is equal to 1.0. σsp is splitting strength of cement stabilized macadam, which is 0.5 MPa. A, B are anti-tensile strength structural coefficients, which take 0.35, 0.11, respectively. σ is bottom tensile stress, MPa. The fatigue life of the pavement structure can be calculated by Eqs. (15) and (16), which is shown as Fig. 9. For Structure 1, Structure 2, and Structure 3, from Fig. 7, it can be seen that compared with the original design structure, the fatigue life of the optimized pavement structure back-calculated by the deflection increased by 220.8%, 186.8%, and 6.4%, respectively. The fatigue life

back-calculated by the bottom tensile stress increased by 154.9%, 364.1%, and 82.1%, respectively. The related research showed that the bottom tensile strain decreases with the increase of base course modulus, thereby increasing the asphalt pavement's fatigue life [33]. The modulus of the optimized pavement structure is increased, which improves the overall pavement structure's ability to resist deflection, thereby increasing the pavement structure's service life.

5.2.2. Fatigue life prediction results based on normalized fatigue equation

In the previous research, the research team determined a normalized fatigue equation for different stress states of cement stabilized macadam

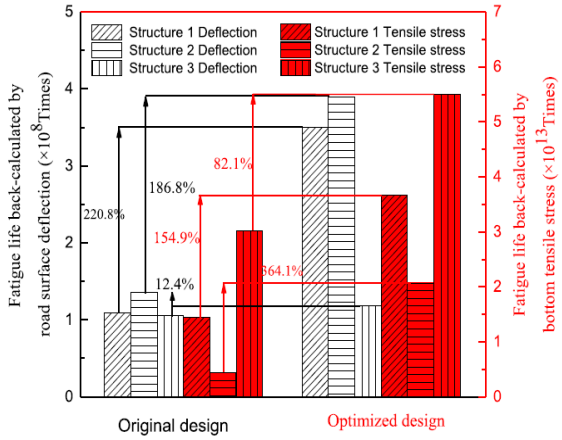

Fig. 9. The fatigue life of three pavement structures based on deflection and bottom tensile stress

based on the idea of yield criterion [34–36]. The loading rate v can be calculated by the stress level σ applied in the fatigue test, and the loading frequency f. The equation is as follows.

$$v = 2\sigma f \tag{17}$$

In this paper, the mathematical model of strength S and loading rate v selected is as follows.

$$S = 0.641v^{0.302} \tag{18}$$

Based on the Desai yield surface response model, the strength yield surface coordinates of the material in a stress-invariant space are determined as ($I1$, $\sqrt{J2}$). In this middle, $I1 = \sigma$, $\sqrt{J2} = \sqrt{3}\sqrt{3}\,\sigma$. Failure shear stress intensity is $\sqrt{J2Nf} = \sqrt{3}\sqrt{3}\,S$. The value of the fatigue resistance of cement stabilized macadam material is the ratio of the initial stress intensity to the shear stress intensity, which is expressed by Δ. The equation is as follows.

$$\Delta = \frac{\sqrt{J_2}}{\sqrt{J_{2N_f}}} \tag{19}$$

The corresponding relationship between fatigue failure resistance Δ and fatigue life Nf can be established. The normalized fatigue equation of cement stabilized macadam under different stress states are created, and the corresponding relationship is as follows.

$$N_f = \Delta^{-10.1858} \tag{20}$$

According to subsection 4.1, for Structure 1, Structure 2, and Structure 3, the bottom tensile stress of the base course before the optimization is 0.051 MPa, 0.058 MPa, and 0.047 MPa, respectively. The bottom tensile stress of the base course after optimization is 0.046 MPa, 0.049 MPa, and 0.044 MPa, respectively. Based on the normalized fatigue equation, the fatigue life of the pavement structure before and after optimization can be obtained. The results are shown in Fig. 10. For Structure 1, Structure 2, and Structure 3, from Fig. 10, it can be seen that compared with the original design structure, the fatigue life of the optimized pavement structure calculated by the normalized fatigue equation increased by 108.38%, 230.85%, and 59.87%, respectively. The above comprehensive analysis shows that the fatigue life of the pavement structure is unified by establishing the relationship between the shear failure capacity and the fatigue life, and by back-calculating the fatigue life through the deflection and the bottom tensile stress. After optimization, the stress on the pavement structure has been significantly improved, and the fatigue life has been substantially improved. The feasibility of the pavement structure modulus optimization has been verified. The asphalt pavement structure design should adopt the appropriate softening method. The base course modulus should be reasonably reduced, which should coordinate with the cushion layer and the subgrade modulus. Meanwhile, the base course and surface course should have a reasonable modulus matching. It can reduce early damage to the pavement. This method has a positive effect on improving the fatigue life of the roadway.

5.2.3. Service life prediction of the pavement structure

To further verify the feasibility of a balanced and coordinated modulus of the semi-rigid base pavement structure, the service life of the pavement structure is estimated. The optimized pavement structure with minimum fatigue life is an example. The fatigue life of the pavement structure before modulus optimization is 6.7 × 1010 times according to fatigue normalization equation. The pavement structure with the minimum fatigue life after optimization is Structure 2. The fatigue life calculated by utilizing the normalized fatigue equation is 2.22 × 1011 times. The cumulative number of axle loads can be calculated by Eq. (21) based on the daily average equivalent axle loads of the design lanes in the initial year, the design service life, etc.

$$N_e = \frac{[(1+\gamma)^t - 1] \times 365}{\gamma} N_1 \quad (21)$$

In the formula: *Ne* is the designed axle load cumulative loads during the design service life, times. γ is the average annual growth rate of traffic volume, %. *t* is the service life, year. *N*1 is the design axle load daily action, times; According to the data query [37,38], diurnal action times of the design axle load are taken at 16,541 times / d, and the annual average growth rate of the traffic volume during the design life is taken at 14.8%, the cumulative number of axles loads is 6.7 × 1010 times and 2.22 × 1011 times. The service life of pavement structure before modulus optimization is 37 years. The service life of the semi-rigid base asphalt pavement can be up to 62 years. It can be learned from this fact that the balanced coordination of the modulus of the semi-rigid base course can improve the fatigue life of the pavement structure, which can become a long-life structure.

6. Conclusions

According to the results obtained in this study, the following conclusions can be drawn:

(1) The laboratory test modulus and the field modulus of pavement structure were measured as the parameters. The mechanical properties of the pavement structure are compared and analyzed. A graded broken stone stiffness transition layer was set between the subbase and the subgrade. On the one hand, it can effectively compensate for the stiffness of the subgrade. On the other hand, it can make the entire pavement structure have rigidity transition, reasonable stress, and harmonious deformation. Thereby, the bottom tensile stress of the semi-rigid base can be reduced effectively.

(2) From the mechanical point of view, each factor's influence level on the pavement mechanical response index was calculated and analyzed. The semi-rigid base pavement structure was optimized based on the balanced and coordinated design of structural layer modulus. The optimization results significantly reduce the bottom tensile stress and deflection of the semi-rigid base asphalt pavement structure and significantly improve fatigue life.

(3) In this research, the fatigue life of semi-rigid base asphalt pavement was predicted based on deflection and bottom tensile stress, and the laboratory normalized fatigue equation, respectively. The combination of pavement material fatigue property and pavement structure fatigue performance was realized. The prediction results show that the semi-rigid base asphalt pavement is a potential long-life asphalt pavement, and its service life can reach 62 years.

(4) In this study, the semi-rigid base asphalt pavement's mechanical response and fatigue life are systematically analyzed. The unity of material fatigue and structural fatigue is achieved. However, the linear viscoelastic behavior of the asphalt layers, the layers interface, nonlinear distribution of temperature inside the pavement structure are not considered in this research. It will be carried out in the subsequent work. In the future, the influence of different structural combinations, thickness, and dynamic modulus on the mechanical properties of the pavement needs further calculation and analysis to verify the universality and availability of the method and model.

References

[1]. C. Jing, J. Zhang, S. Bo, An innovative evaluation method for performance of in-service asphalt pavement with semi-rigid base, Constr. Build. Mater. 235 (2020) 117376, https://doi.org/10.1016/j.conbuildmat.2019.117376

[2]. D. Liu, Z. Wang, Research on the design of asphalt pavement structure in a hot and rainy area, Heilongjiang Jiaotong Keji (3) (2019) 50-51,53. doi: 10.16402/j.cnki. issn1008-3383.2019.03.028.

[3]. S. Lv, J. Yuan, X. Peng, M. Borges Cabrera, S. Guo, X. Luo, J. Gao, Performance and optimization of bio-oil/Buton rock asphalt composite modified asphalt, Constr. Build. Mater. 264 (2020) 120235, https://doi.org/10.1016/j. conbuildmat.2020.120235.

[4]. C. Raab, M.N. Partl, Interlayer bonding of binder, base and subbase layers of asphalt pavements: Long-term performance, Constr. Build. Mater. 23(8) (2009) 2926-2931. doi: 10.1016/j.conbuildmat.2009.02.025.

[5]. M. Elshaer, J.S. Daniel, Impact of pavement layer properties on the structural performance of inundated flexible pavements, Transp. Geotech. 16 (2018) 11–20.

[6]. C. Xia, S. Lv, M.B. Cabrera, X. Wang, C. Zhang, L. You, Unified characterizing fatigue performance of rubberized asphalt mixtures subjected to different loading modes, J. Cleaner Prod. 279 (2021) 123740, https://doi.org/10.1016/j. jclepro.2020.123740.

[7]. H.J. Lee, J.H. Lee, H.M. Park, Performance evaluation of high modulus asphalt mixtures for long life asphalt pavements, Construction and Building Materials 21 (5) (2007) 1079-1087. doi:

10.1016/j.conbuildmat.2006.01.003.
[8]. N.J. Santero, J. Harvey, A. Horvath, Environmental policy for long-life pavements, Transp. Res. Part D: Transp. Environ. 16(2) (2011) 129-136. doi: 10.1016/j. trd.2010.09.005.
[9]. P.E. Yuhong Wang, Y. Wen, K. Zhao, D. Chong, A.S.T. Wong, Evolution and locational variation of asphalt binder aging in long-life hot-mix asphalt pavements, Constr. Build. Mater. 68 (2014) 172–182.
[10]. S. Lv, C. Xia, H. Liu, L. You, F. Qu, W. Zhong, Y.i. Yang, S. Washko, Strength and fatigue performance for cement-treated aggregate base materials, Int. J. Pavement Eng. 22 (6) (2021) 690–699.
[11]. H.H. Titi, M.G. Matar, Estimating resilient modulus of base aggregates for mechanistic-empirical pavement design and performance evaluation, Transp. Geotech. 17 (2018) 141–153.
[12]. G. Zang, L. Sun, Z. Chen, L.i. Li, A nondestructive evaluation method for semi-rigid base cracking condition of asphalt pavement, Constr. Build. Mater. 162 (2018) 892–897.
[13]. G. Yang, X. Wang, Study on the rationality of application of high modulus asphalt concrete in long-life semi-rigid base asphalt pavement, Journal of Highway and Transportation Research and Development 36(5) (2019) 20-26+56.
[14]. S. Lv, J. Yuan, X. Peng, M. Borges Cabrera, H. Liu, X. Luo, L. You, Standardization to evaluate the lasting capacity of rubberized asphalt mixtures with different testing approaches, Constr. Build. Mater. 269 (2021) 121341, https://doi.org/ 10.1016/j.conbuildmat.2020.121341.
[15]. X. Zhao, Design method of the long-life asphalt pavement structure, China Highway (1) (2019) 104-105. doi: 10.13468/j.cnki.chw.2019.01.033.
[16]. Y. Luo, The influence analysis of structural parameters on the mechanical behavior of asphalt pavement, Shanxi Science and Technology of Communications (3) (2016) 26-28.
[17]. R. Zhang, T. Ling, M. Yuan, H. Ning, Influence of asphalt semi-rigid base modules on pavement structural stress, Journal of Chongqing Jiaotong University(Natural Science) 30(4) (2011) 755-758+863.
[18]. F. Li, L. Sun, Analysis of the influence of base course modulus on the mechanical performance of asphalt pavement, J. Highway Transp. Res. Development 23(10) (2006) 41-43+49.
[19]. X. Ma, Z. Guo, Mechanical analysis of the effect of base course modulus on asphalt pavement performance, J. China Foreign Highway 28(4) (2008) 46-48. doi: 10.14048/j.issn.1671.
[20]. B. Zhou, J. Li, H. Li, G. Qian, Sensitive mechanical analysis of structural parameters of semi-rigid base asphalt pavement, J. China Foreign Highway 27 (4) (2007) 65–69.
[21]. O.C. Assogba, Y. Tan, X. Zhou, C. Zhang, J.N. Anato, Numerical investigation of the mechanical response of semi-rigid base asphalt pavement under traffic load and nonlinear temperature gradient effect, Constr. Build. Mater. 235 (2020) 117406, https://doi.org/10.1016/j.conbuildmat.2019.117406.
[22]. S. Ma, W. Xu, H. Liu, Y. Xu, Reliability analysis of semi-rigid base asphalt pavement structure, J. China Foreign Highway 37 (6) (2017) 77–80.
[23]. D. Li, Analysis of the structural combination optimization of asphalt pavement, Highway Eng. 42(6) (2017) 152-157+260.
[24]. M. Asadi, R.S. Ashtiani, Stability analysis of anisotropic granular base layers in flexible pavements, Transp. Geotech. 14 (2018) 183–189.
[25]. J. Coffey, B. Ghadimi, H. Nikraz, M. Rosano, The modeling prediction of haul road surface deflection, Transp. Geotech. 14 (2018) 136–145, https://doi.org/10.1016/ j.trgeo.2017.11.005.
[26]. P. Tamrakar, S. Nazarian, Evaluation of plate load based testing approaches in measuring stiffness parameters of pavement bases, Transp. Geotech. 16 (2018) 43–5
[27]. T.J. Barrett, M. Knezevic, Deep drawing simulations using the finite element method embedding a multi-level crystal plasticity constitutive law: Experimental verification and sensitivity analysis, Comput. Methods Appl. Mech. Eng. 354 (2019) 245–270.
[28]. X. Chen, H. Li, Research three-dimensional finite element model of asphalt pavement structure, J. Wuhan Univ. Technol. 44 (3) (2020) 584–590.
[29]. N. Chrisochoides, D. Nave, Simultaneous mesh generation and partitioning for Delaunay meshes, Math. Comput. Simul 54 (2000) 321–339.
[30]. H. Li, J. Wu, J. Liu, Y. Liang, Finite element mesh generation and decision criteria of mesh quality, China Mech. Eng, 23 (3) (2012) 368–377.
[31]. JTG D50-2006, Specifications for Design of Highwat Asphalt Pavement, Renmin Communication Press, Beijing, China (2006).
[32]. S. Wu, H. Chen, J. Zhang, Z. Zhang, Effects of interlayer bonding conditions between semi-rigid base layer and asphalt layer on mechanical responses of the asphalt pavement structure, International Journal of Pavement Research and Technology 10(3) (2017) 274-281. doi: 10.1016/j.ijprt.2017.02.003.
[33]. D. Wei, Disress Mode and Structure Optimization of Asphalt Pavement with Semi-rigid Base, PhD thesis, Changan Universtity, Xi'an, China, 2010.
[34]. C. Liu, S. Lv, D. Jin, F. Qu, Laboratory investigation for the road performance of asphalt mixtures modified by rock asphalt/styrene butadiene rubber, J. Mater. Civ. Eng. (2020), https://doi.org/10.1061/(ASCE)MT.1943-5533.0003611.
[35]. S. Lv, C. Liu, D. Chen, J. Zheng, Z. You, L. You, Normalization of fatigue characteristics for asphalt mixtures under different stress states, Constr. Build. Mater. 177 (2018) 33–42.
[36]. C. Liu, S. Lv, X. Peng, J. Zheng, Normalized characterization method for fatigue behavior of cement-treated aggregates based on the yield criterion, Constr. Build. Mater. 228 (2019) 117099, https://doi.org/10.1016/j.conbuildmat.2019.117099.
[37]. Development and Reform Commission of Zhangzhou, Feasibility Study Report on Xiamen-Zhangzhou Expressway, https://www.docin.com/p-952941965-f4.html (2006).
[38]. Department of Transportation of Hunan Province, Statistical communiqu´e on the development of hunan highway and waterway transportation industry in 2018, http://jtt.hunan.gov.cn/xxgk/jttj/201904/t20190416_5316077.html (2019).
[39]. J. Jin, S. Liu, Y. Gao, et al., Fabrication of cooling asphalt pavement by novel material and its thermodynamics model, Constr. Build. Mater. (2021), 121930, https://doi.org/10.1016/j.conbuildmat.2020.121930.
[40]. M. Liao, Z. Liu, Y. Gao, et al., Study on UV aging resistance of nano-TiO2/ montmorillonite/styrene-butadiene rubber composite modified asphalt based on rheological and microscopic properties, Constr. and Build. Mater. (2021), 124108, https://doi.org/10.1016/j.conbuildmat.2021.124108.